DOI:
10.1038/ki.2012.264

Document Version
Peer reviewed version

Probenecid prevents acute tubular necrosis in a mouse model of aristolochic acid nephropathy

Thomas Baudoux [1], Agnieszka A. Pozdzik [1,2*], Volker M. Arlt [3], Eric De Prez [1],Marie-Hélène Antoine[1], Nathalie Quellard [4], Jean-Michel Goujon [4], Joëlle L. Nortier [1,2]*

[1]Experimental Nephrology Unit, Faculty of Medicine; [2]Nephrology Department, Erasme Hospital, Université Libre de Bruxelles, Brussels, Belgium; [3]Analytical and Environmental Sciences Division, MRC-HPA Centre for Environment & Health, King's College London, London, UK; [4]Department of Pathology & Electron Microscopy, CHU La Miletrie, Poitiers, France and INSERM U 1082, Poitiers, France

[*] These authors contributed equally to this work

T.B. is a research fellow in Nephrology at the Université Libre de Bruxelles (Belgium) and research associate with Erasme Foundation (Erasme Hospital, Brussels, Belgium)

Running headline: Protective effects of probenecid in AAN

Subject of manuscript: Physiopathology of renal disease and progression

Words count: 3653

Corresponding author:

Joëlle L. NORTIER, MD, PhD

Nephrology Dept, Erasme Hospital, Université Libre de Bruxelles

Route de Lennik 808, B- 1070 Brussels, Belgium

Phone: + 32-2-555-3334, Fax: +32-2-555-6499,

E-mail: Joëlle.Nortier@erasme.ulb.ac.be

ABSTRACT

Experimental aristolochic acid nephropathy (AAN) is characterized by early tubulo-interstitial (TI) injury (necrosis of proximal tubular epithelial cells (PTEC) and inflammatory infiltrate). It also reproduces chronic lesions seen in humans (tubular atrophy and interstitial fibrosis). *In vitro***,** probenecid (PBN) inhibits AA entry through organic anion transporters (OATs), reduces specific AA-DNA adduct formation and preserves cellular viability. To confirm these results *in vivo*, we reproduced experimental AAN in a mouse model. Plasma creatinine level (Pcr), tubulo-interstitial (TI) lesions, DNA repair processes (proliferating cell nuclear antigen tissue expression) and AA-DNA adduct formation were studied. AA induced severe TI injuries (necrosis of PTEC followed by mononuclear cells infiltration, tubular atrophy and an interstitial fibrosis) and transient acute kidney injury. Addition of PBN prevented Pcr increase, TI injuries and reduced both the extent and the severity of ultrastructural lesions induced by AA (loss of brush border, mitochondrial edema and disappearance of mitochondrial crests). Further, PCNA positive cells count and total AA-DNA adduct levels were significantly reduced in mice receiving AA+PBN compared to mice treated with AA alone. The present data demonstrate in vivo the nephroprotective effect of PBN, an OATs inhibitor, towards acute PTEC toxicity in a mouse model of AAN.

KEYWORDS

Aristolochic acid nephropathy

Proximal tubular epithelial cells

Probenecid

Acute tubular necrosis

Interstitial renal fibrosis

DNA adducts

ABBREVIATIONS

AA; Aristolochic acid

AAN; Aristolochic acid nephropathy

TI; Tubulointerstitial

PTEC; Proximal tubular epithelial cell

α-SMA; α-Smooth Muscle Actin

Pcr; Plasma creatinine

Mn/Mϕ; Monocytes/Macrophages

NEP; Neutral endopeptidase

OA; Organic anion

OAT; Organic anion transporter

PBN; Probenecid

PCNA; Proliferating Cell Nuclear Antigen

PEG; Polyethylene glycol

INTRODUCTION

Human aristolochic acid nephropathy (AAN) is a tubulointerstitial (TI) nephritis reported after intake of herbal remedies containing aristolochic acid (AA). (1, 2) It is histologically characterized by a typical corticomedullary gradient of interstitial fibrosis and the progressive atrophy of proximal tubules, resulting in the rapid deterioration of renal function to the end-stage. (3, 4) AA intoxication also leads to the formation of specific AA-DNA adducts which are premutagenic lesions involved in the development of AAN-associated urothelial cancer and their long-term presence in renal tissue is used as a biomarker of AA exposure. (5, 6)

AA-induced TI nephritis was experimentally reproduced in rabbits, mice and rats (7-10). A biphasic evolution of TI lesions was identified in our Wistar rat model. (11, 12) In the early, so-called *acute phase*, a transient tubular necrosis located in the S3 segment (proximal tubular epithelial cells (PTECs)) and a mononuclear cell infiltration are observed; later, in the so-called *chronic phase*, tubular atrophy and interstitial fibrosis are clearly the prominent features. In this step-by-step model, inflammatory cells were proposed as the physiopathological link between both phases. (11) *In vitro* data early confirmed that PTEC were the target of AA (13), suggesting the presence of specific molecular mechanisms responsible for the accumulation of AA in PTECs. The excretion of numerous organic anions (OAs) including endogenous metabolites through PTECs is actually achieved via unidirectional transcellular transport, involving the uptake of OAs from the blood across at the basolateral membrane and their extrusion across the apical membrane into the tubular lumen. Organic anion transporters (OATs) play a key role in this process. At least eleven isoforms of OATs have been identified; a majority of them was found in the kidney. OATs are exchangers linked to two other transporters, the

sodium dicarboxylate cotransporter and the sodium-potassium ATPase. OA are taken up by OAT 1 and/or 3 in the basolateral membrane of the proximal tubule. This uptake is processed in parallel to the countertransport of α-ketoglutarate. The drug then crosses the cell and is excreted in the lumen of the tubule. (14, 15) The activity of OATs has been associated with proximal tubular injury due to the accumulation of toxics, such as uremic toxins, drugs and mercuric species. (14-17) In embryonic kidney cells (HEK293) as well as *Xenopus laevis* oocytes, three human isoforms (OAT1, OAT3 or OAT4) were reported to play a role in intracellular accumulation of AA. (18, 19) Moreover, probenecid (PBN) blocked AA entry by inhibition of human OATs, reducing the formation of AA-DNA adduct (19), and preserved cell viability. (18)

We investigated this last aspect *in vivo* in a mouse model of AAN. We hypothetized that PBN, by reducing AA entry through OATs, could protect PTECs against lesions, preventing AA-DNA adduct formation and thus preserve cell viability.

RESULTS

Ninety-six mice C57BL/6 were randomly assigned to 4 groups of 24 animals each. According to group, mice were injected with AA, AA+PBN or solvent (polyethylene-glycol (PEG))+PBN. Control group was injected with PEG (Figure 1). AA (5 mg/kg body weight) or PEG was injected once a day and PBN (150 mg/kg body weight) twice a day. These dosing regimens of PBN have been shown to inhibit organic anion transporter (20)

Plasma creatinine level (Pcr), TI lesions, DNA repair processes (proliferating cell nuclear antigen tissue expression) and AA-DNA adduct formation were quantified in each group after 2, 4, 5 and 8 days of AA injections.

Probenecid prevents AA-induced acute kidney injury

A transient acute kidney injury, as reflected by significant increase in Pcr levels was observed in mice receiving AA after 5 days of injections as compared to control animals [PCr (mg/dl), median (min-max): 0.353 (0.222-0.504) *vs* 0.135 (0.112-0.211); $p<0.0022$]. Addition of PBN prevents Pcr increase in AA animals [PCr (mg/dl), median (min-max): 0.125 (0.105-0.139) vs 0.353 (0.222-0.504); $p<0.0022$]. No significant change in Pcr levels was measured in PEG+PBN group as compared to controls (Figure 2).

Probenecid significantly reduces AA-induced TI injury

As demonstrated in Figures 3-4a-d and 3-4e-h, the renal parenchyma from PEG and PEG+PBN groups remained normal in optical microscopy analyses at all studied time points of protocol. In contrast, early histological lesions were present in the AA group (Figures 3-4i-l). As early as day 2, a swelling of PTEC was found in the medullary rays (Figure 4i). In the same areas, prominent PTEC necrosis was observed at days 4 and 5 (Figures 3-4j-k). After 8 days of AA treatment, tubular atrophy was clearly widespread as reflected by dilatation and flattening of PTECs as well as tubular basement membrane thickening. In the surrounding interstitial areas, mononuclear cells infiltration was observed at day 4 and progressively extended to day 8. At that time point, this inflammatory process was associated with extracellular matrix deposition. In mice receiving AA+PBN, swelling and necrosis of PTECs was limited to few tubules located in the medullary rays only at day 4 without any interstitial inflammatory cells infiltration (Figures 3-4n). Moreover, proximal tubules as well as the surrounding interstitial areas appeared normal under optical microscopy analysis at days 5 and 8 (Figure 3-4o-p).

Throughout the protocol, no abnormality was detected within the glomeruli from all groups under optical microscopy analysis.

As compared with controls, the semiquantitative score of TI injury obtained in AA-treated mice revealed tubular necrosis from day 4 to 8 with an evident peak at day 5 (Figure 5a), lymphocytic infiltration from day 5 (Figure 5b), marked tubular atrophy at day 5 accompanied by progressive interstitial fibrosis (Figure 5c and 5d, respectively). In the AA+PBN group, a significant reduction of all the semiquantitative scores was found: of tubular necrosis on days 5 ($p<0.0013$) and 8 ($p<0.0025$)), of lymphocytic infiltrate ($p<0.0013$) and of tubular atrophy ($p<0.0018$) (day 8) as well as of interstitial fibrosis on days 5 ($p<0.0022$) and 8 ($p<0.0013$) (Figure 5a-d).

Necrosis of positive neutral endopeptidase tubules is prevented by PBN

To further assess the distribution of necrotic tubules, an immunostaining of neutral endopeptidase (NEP) was performed and evaluated. NEP is a specific marker for the brush border of S3 segment of the proximal tubule in rat. (21) As shown in Figure 6, immunostaining of NEP in control groups demonstrated that NEP positive cells were mainly located in medullary rays and in the outer stripe of outer medulla, reproducing the typical distribution of NEP positive cells in *pars recta* of proximal tubule observed previously in our rat model (11, 22). No disappearance of NEP immunostaining was observed in PEG or PEG+PBN groups. AA administration lead to a progressive necrosis of PTECs, especially NEP positive as suggested by the progressive disappearance of NEP staining in the medullary rays and the presence of intratubular necrotic NEP positive cells on day 5 (Figure 6c). At day 8, NEP positive cells had completely disappeared from medullary rays (Figure 6d). On the contrary, NEP immunostaining was maintained in the AA+PBN group (Figure 6e,f).

Addition of PBN leads only to a mild reduction of AA-DNA adduct formation

As PBN administration was effective in significantly preventing acute kidney injury and TI lesions induced by AA, we examined possible effect of PBN on AA-DNA adduct formation in kidney cortex tissue samples. As shown in Figure 7a, the pattern of AA-DNA adducts consisted of three major adduct spots: 7-(deoxyadenosin-N^6-yl)-aristolactam I (dA-AAI, spot 1), 7-(deoxyguanosin-N^2-yl)-aristolactam I (dG-AAI, spot 2) and 7-(deoxyadenosin-N^6-yl) aristolactam II (dA-AAII, spot 3). This pattern is identical to those observed previously in our rat model and in AA-exposed patients. (6, 22)

In the AA+PBN group, as compared to the AA group, there were no significant changes in AA-DNA adducts at days 2,4 and 5, while a significant reduction of the total AA-DNA adduct levels was observed at day 8 (Figure 7b). There was no correlation between the Pcr levels or the TI scores and AA-DNA adduct formation (data not shown).

Previous in vivo studies showed that DNA adduct formation by AA reaches a steady-state level which is likely the result of a balance between adduct formation and their loss through either DNA-repair processes or apoptosis. (22, 23) Moreover, this level seems to reached quickly, even 2 days after the first injection in a rat model. (22) This could explain the only small differences in DNA adduct levels between the two groups after 8 days of treatment. Therefore, we conducted an additional experiment to investigate the early time course and kinetic of AA-DNA adduct formation. Thirty-two mice were injected with AA or AA+PBN as previously and 4 mice per group were sacrificed after 6, 12, 18 and 24 hours. At these time points, differences in AA-specific DNA adduct levels between the two groups were clearly observed (Figure 7a) confirming that PBN significantly inhibits AA-DNA adduct formation.

PBN significantly reduces AA-induced DNA damage repair processes and cell proliferation attested by PCNA immunostaining

PCNA is a polymerase cofactor, involved in DNA damage repair processes and in the stability of the DNA microsatellite region. (24) Only few tubular cells expressed PCNA in controls (PEG and PEG+PBN groups) (Figure 8a-h). In AA-treated mice, typical nuclear patterns of PCNA immunostaining were predominantly seen in PTECs and less frequently in interstitial cells from the corticomedullary junction as soon as day 2 and still increased until day 8 (Figure 8i-l). PBN administration resulted in a reduction of PCNA expression induced by AA in mice as soon as day 4 (Figure 8m-p).

As compared to controls, the proportion of PCNA positively stained areas per field was higher in AA-treated mice from day 5 ($p<0.0043$) to day 8 ($p<0.0152$) (Figure 8q). This proportion was significantly decreased in the AA+PBN group at day 5 ($p<0.0043$) and day 8 ($p<0.0022$) (Figure 8q).

PBN reduces the degree of ultrastructural lesions of PTEC induced by AA

Control groups (PEG and PEG+PBN) exhibited only mild mitochondrial swelling in few PTEC at day 8 (Figure 9a,b). In kidneys from AA-treated mice, considerable variation in the degree of cellular damage may occur. Normal tubules were frequently admixed with injured nephron showing extensive mitochondria disruption and altered brush borders (Figure 9c,e). PBN administration reduced both the extent and the severity of cellular damage induced by AA (Figure 9d,f).

DISCUSSION

Since the cluster outbreak of the so-called Chinese herbs nephropathy in 1993,

AAN is now recognized as a public health problem worldwide (25): it is identified as an environmental kidney disease in the Balkan region and probably underestimated in Asian countries where traditional Chinese medicine is widely used, as suggested by two recent studies. (26, 27) Understanding its physiopathology may lead to effective therapies preventing the progression of chronic kidney disease.

In the present study, we reproduced histopathological features of human AAN (tubular necrosis, inflammatory interstitial infiltrate, tubular atrophy and interstitial fibrosis) in a short-term mouse model. Male C57BL/6 mice were injected daily with a mixture of AAI and AAII, the same as the one present in *Aristolochia sp.* and ingested by our patients. After 4 days of injection, a massive necrosis of PTEC from the medullary rays was observed, resulting in an acute kidney injury on day 5. This "acute" phase was followed by a prominent atrophy and fibrosis on day 8. The normalization of creatinine on day 8 is consistent with our observations of the acute phase in the AAN rat model in which a transient creatinine increase on day 5 was followed by a normalization of creatinine on day 8, contrasting with persistent histological lesions. (22) In addition, such dissociation between plasma creatinine and histology during the recovery phase has been described in other models of acute kidney injury like ischemia and reperfusion. (28)

The addition of PBN prevented acute kidney injury and significantly reduced tubular necrosis, lymphocytic infiltrate, atrophy and fibrosis. Moreover, immunohistochemical study using PCNA staining confirmed the protective effect of PBN from AA. Increase in PCNA staining reflects a proliferation process of PTECs secondary to necrosis, which is in accordance with previous histological findings obtained in our rat model using Ki67 immunostaining. (12) Finally, a reduction of AA-DNA adduct formation was found in mice receiving AA+PBN as compared to mice treated with AA

alone.

Recently, two *in vitro* studies demonstrated that PBN inhibits AA entry in human OAT-transfected HEK293 kidney cell lines (19) and in human OAT-transfected cell lines derived from the second portion of the proximal tubule. (18) Further, the former study indicated that PBN can reduce AA-DNA adduct formation and that addition of PBN to AA preserved cellular viability. The present work brings significant *in vivo* results confirming the protective effects of PBN against AA-induced TI lesions by blocking AA entry into PTEC via OATs. Actually, these histomorphometric data can be related to a recent pharmacological study focusing on the effects of PBN on AA liver and kidney metabolism. (29) These authors reported a significantly reduced accumulation of renal AAI in mice exposed to AA and PBN as well as an increase in AAI liver content and biliary clearance.

Regarding the evident protective effect of PBN in terms of TI AA-induced lesions, it could be surprising to measure a only slight, difference of AA-DNA adduct level between AA and AA+PBN group. However, this discrepancy could be easily interpreted. First of all, in AA+PBN group, AA may enter PTEC independently of OAT. Other endogenous transmembrane transporters or passive diffusion may also be involved in the uptake of AA, as suggested by a only partial blockade of AA entry by PBN in an *in vitro* model of human OAT-transfected HEK293 cells (19). Secondly, DNA adduct formation by AA often quickly reaches a steady-state level as seen in previous in vivo studies and our present results. In addition, our data suggest that although AA-DNA adducts are a clue biomarker of AA exposure, there is no correlation between AA-specific DNA adduct levels and nephrotoxicity.

Dissociation between AA-mediated nephrotoxicity and adduct formation was first suggested by a clinical case report of AA-induced tumor development without renal

impairment. (30) This observation was followed by two rodent studies showing that AA-DNA adducts were the basis for the carcinogenic effect of AA but were unrelated to nephrotoxic insult. Indeed, both AAI and AAII could cause similar types of DNA damage (i.e. bulky DNA adducts) whereas only AAI is nephrotoxic *in vivo*. (9, 10) *In vitro* studies confirmed that AAI is much more cytotoxic compared to AAII due to the presence of a methoxy group in position 8. (31, 32) On the other hand, the carboxyl group rather than the nitro group is important to facilitate AA entry into tubular cells via OATs. Finally, nitroreduction results in *N*-hydroxy-aristolactam formation and these metabolites bind covalently to the exocyclic amino groups of adenine or guanine forming AA-specific DNA adducts. (33, 34) On the other hand, AAI seems to directly cause renal injury by activating mitochondrial permeability transition (35), and reticulum endoplasmic stress. (36) Further, AA is responsible for increased oxidative stress-related DNA lesions due to glutathione depletions (37) and AA can block DNA replication causing cycle arrest and/or apoptosis in renal epithelial cells *in vitro* and *in vivo*. (38-40)

In conclusion, we developed an *in vivo* model of AAN characterized by an early episode of acute kidney injury induced by daily injections of AA. Despite highly nephrotoxic effects of AA, we were able to demonstrate a sustained protective effect of PBN by blocking AA entry into PTEC and then preventing acute tubular necrosis.

METHODS

Experimental protocols

All procedures were in accordance with the Ethical Committee for Animal Care (Faculty of Medicine, Université Libre de Bruxelles). After one week of acclimatization, 10 weeks old C57BL/6 male mice, n=96 (Elevage Janvier, Le Genest Saint-Isle, France) were

randomly assigned to 4 groups of 24 mice each and were injected ip with solvent (polyethylene glycol (PEG group)) alone; PEG+PBN (4-[(dipropylamino)sulfonyl]benzoic acid) (PEG group); AA (AA group) or AA+PBN (AA+PBN group). AA (Acros Organics Co., Geel, Belgium; 40% AAI, 60% AAII,) was dissolved in PEG (Fluka Chemie, Buchs, Switzerland). PBN (Sigma-Aldrich, Bornem Belgium) was solubilized in NaOH 0.5 M at 45°C for 10 min then diluted with PBS and buffered to 7.4 with HCl. AA (5 mg/kg body weight) or equivalent volume of PEG were given once a day and PBN (150 mg/kg body weight) twice a day. AA was given once a day ip in 150 µl of solvent and PBN (150 mg/kg body weight) was injected with 150 µl of PBS twice a day for a total of 8 days maximum. After 2, 4, 5 or 8 days of injection, 6 mice per group were sacrificed. After intraperitoneal anesthesia with ketamine-HCl (Merial, Brussels, Belgium) and 2% xylazine (Bayer, Brussels, Belgium), a blood specimen was obtained by cardiac puncture and kidneys were harvested for analysis. Different samples of kidneys were fixed. One part in alcohol-formalin-acetic for optical microscopy, one in 4% buffered formaldehyde for immunohistochemistry, one in glutaraldehyde sodium cacodylate buffer for electron microscopy analysis and one frozen in liquid nitrogen and stored at –80°C for subsequent DNA adduct analysis.

Renal histopathology

TI injury semiquantification was evaluated on hematoxylin/eosin and Masson's trichrome-stained paraffin-embedded sections. Complete kidney sections were analyzed with a light microscope (Carl Zeiss, Oberkochen, Germany) using a 20× magnification lens by two investigators (AAP and TB) blind to the group origin of the mice. The scoring systems were defined as previously described (11, 12): tubular necrosis: 0, normal tubules; 1, rare single necrotic tubule; 2, several clusters of necrotic tubules; 3,

confluence of necrotic clusters; tubular atrophy: 0, normal tubules; 1, rare single atrophic tubule; 2, several clusters of atrophic tubules; 3, confluence of atrophic tubular clusters; lymphocytic infiltrate: 0, absent; 1, few scattered cells; 2, group of lymphocytes; 3, widespread infiltrate; interstitial fibrosis: 0, absent; 1, minimal fibrosis; 2, moderate fibrosis; 3, severe fibrosis. If differences in grading occurred, the appropriate sections were re-examined until a consensus was obtained.

Biochemical evaluation of renal function

Plasma creatinine (Pcr) excretion levels were determined as previously described using an HPLC technique. (11, 12)

Immunohistochemistry

The FFPE sections (4 µm) were attached to poly-L-lysine pretreated slides (Sigma-Aldrich, Bornem, Belgium). After air-drying the paraffin from FFPE tissue sections was removed (xylene solution). The sections were rehydrated and immersed in a retrieval solution, sodium citrate buffer (pH 6.0), the microwave oven technique was used (650 W, 1×5 min). PBS was used for all washing steps. Endogenous peroxidase activity was quenched with 0.3% hydrogen peroxide in a methanol solution (30 min). Non-specific protein binding sites (background staining due to Fc receptor) were blocked with 20% normal serum (Vectastain Elite_ABC kit IgG, Vector Laboratories, Labconsult, Brussels, Belgium) then with avidin D solution and with biotin solution (Avidin/biotin blocking kit, Vector Laboratories). Subsequently, the sections were incubated overnight with rabbit anti-mouse PCNA (1/4000) monoclonal primary antibody (Abcam, ab2426) or with rat monoclonal antibody anti NEP (1/4000) (Santacruz, sc-80021) diluted in the blocking buffer. Slides were then incubated with specific biotinylated secondary

antibody (Vectastain Elite_ABC kit, Vector Laboratories, Labconsult, Brussels, Belgium). The extent of the specifically bound primary antibodies was visualized by means of the avidin-biotin peroxidase complex (ABC) method. The diaminobenzidine/hydrogen peroxide was used as the chromogene substrate producing a brown end product. Counterstaining with haematoxylin completed the processing. The specificity of antibodies used was established by the producer. Normal serum (5% solution) instead of the primary antibody (used in order to exclude non-specific staining of kit reagents) showed no staining.

Quantification of PCNA immunostainings

Quantifications were performed by one investigator (TB) blind to the group origin of the mice using ImageJ, a public domain Java image processing program (U.S. NIH) software (available at http://rsb.info.nih.gov/ij) as detailed in Figure 10. Thresholding conditions were set identically for all images. Finally the percentage of DAB positive surface corresponding to DAB-positive cells were counted using ImageJ analyse particle command.

Ultrastructural analysis

Analysis of cellular ultrastructure using transmission electron microscopy was performed in the same period. Small pieces of renal tissue were fixed in 3% glutaraldehyde in 0.1 mol/L phosphate buffer, pH 7.2, Fixation was performed with the microwave oven technique, After rinsing, samples were post-fixed in 1% osmium tetroxide in phosphate buffer 0.1 M for 1 h at 4°C, processed through a graded acetone series, embedded in Araldite (TAAB Laboratories England UK), and polymerized overnight at 60°C. Sections (50 nm) were then stained with uranyl acetate and lead

citrate and examined with a 10-10 JEOL electron microscopy (JEOL, Tokyo, Japan).

AA-DNA adduct analysis

DNA was extracted from frozen tissues using a standard phenol-chloroform extraction method. ^{32}P-postlabelling anaylsis (41) nuclease P1 enrichment, chromatography on polyethyleneimine-cellulose thin-layer plates (Machery and Nagel, Düren, Germany), autoradiography using a Packard Instant Imager (Canberra Co., Dowers Grove, IL, USA) and quantitation were essentially performed as described. (42) Results were expressed as DNA adducts per 10^8 normal nucleotides.

Statistical analysis

All the scores and data obtained from AA and control groups were compared for each corresponding time point with Kruskall-Wallis test followed by Mann-Whitney U-test and Bonferroni post-hoc test.

DISCLOSURE

All the authors declared no competing interests.

REFERENCES

1. Vanherweghem JL, Depierreux M, Tielemans C*, et al.* Rapidly progressive interstitial renal fibrosis in young women: association with slimming regimen including Chinese herbs. *Lancet* 1993; **341:** 387-391.

2. Vanhaelen M, Vanhaelen-Fastre R, But P*, et al.* Identification of aristolochic acid in Chinese herbs. *Lancet* 1994; **343:** 174.

3. Depierreux M, Van Damme B, Vanden Houte K*, et al.* Pathologic aspects of a newly described nephropathy related to the prolonged use of Chinese herbs. *Am J Kidney Dis* 1994; **24:** 172-180.

4. Cosyns JP, Jadoul M, Squifflet JP*, et al.* Chinese herbs nephropathy: a clue to Balkan endemic nephropathy? *Kidney Int* 1994; **45:** 1680-1688.

5. Schmeiser HH, Bieler CA, Wiessler M*, et al.* Detection of DNA adducts formed by aristolochic acid in renal tissue from patients with Chinese herbs nephropathy. *Cancer Res* 1996; **56:** 2025-2028.

6. Nortier JL, Martinez MC, Schmeiser HH*, et al.* Urothelial carcinoma associated with the use of a Chinese herb (Aristolochia fangchi). *N Engl J Med* 2000; **342:** 1686-1692.

7. Cosyns JP, Dehoux JP, Guiot Y*, et al.* Chronic aristolochic acid toxicity in rabbits: a model of Chinese herbs nephropathy? *Kidney Int* 2001; **59:** 2164-2173.

8. Debelle FD, Nortier JL, De Prez EG*, et al.* Aristolochic acids induce chronic renal failure with interstitial fibrosis in salt-depleted rats. *J Am Soc Nephrol* 2002; **13:** 431-436.

9. Sato N, Takahashi D, Chen SM*, et al.* Acute nephrotoxicity of aristolochic acids in mice. *J Pharm Pharmacol* 2004; **56:** 221-229.

10. Shibutani S, Dong H, Suzuki N*, et al.* Selective toxicity of aristolochic acids I and II. *Drug Metab Dispos* 2007; **35:** 1217-1222.

11. Pozdzik AA, Salmon IJ, Husson CP*, et al.* Patterns of interstitial inflammation during the evolution of renal injury in experimental aristolochic acid nephropathy. *Nephrol Dial Transplant* 2008; **23:** 2480-2491.

12. Pozdzik AA, Salmon IJ, Debelle FD*, et al.* Aristolochic acid induces proximal tubule apoptosis and epithelial to mesenchymal transformation. *Kidney Int* 2008; **73:** 595-607.

13. Lebeau C, Arlt VM, Schmeiser HH*, et al.* Aristolochic acid impedes endocytosis and induces DNA adducts in proximal tubule cells. *Kidney Int* 2001; **60:** 1332-1342.

14. Ahn SY, Nigam SK. Toward a systems level understanding of organic anion and other multispecific drug transporters: a remote sensing and signaling hypothesis. *Mol Pharmacol* 2009; **76:** 481-490.

15. Nigam SK, Bush KT, Bhatnagar V. Drug and toxicant handling by the OAT organic anion transporters in the kidney and other tissues. *Nat Clin Pract Nephrol* 2007; **3:** 443-448.

16. Ho ES, Lin DC, Mendel DB*, et al.* Cytotoxicity of antiviral nucleotides adefovir and cidofovir is induced by the expression of human renal organic anion transporter 1. *J Am Soc Nephrol* 2000; **11:** 383-393.

17. Torres AM, Dnyanmote AV, Bush KT*, et al.* Deletion of multispecific organic anion transporter Oat1/Slc22a6 protects against mercury-induced kidney injury. *J Biol Chem* 2011; **286:** 26391-26395.

18. Babu E, Takeda M, Nishida R*, et al.* Interactions of human organic anion transporters with aristolochic acids. *J Pharmacol Sci* 2010; **113:** 192-196.

19. Bakhiya N, Arlt VM, Bahn A*, et al.* Molecular evidence for an involvement of organic anion transporters (OATs) in aristolochic acid nephropathy. *Toxicology* 2009; **264:** 74-79.

20. Emeigh Hart SG, Wyand DS, Khairallah EA*, et al.* Acetaminophen nephrotoxicity in the CD-1 mouse. II. Protection by probenecid and AT-125 without diminution of renal covalent binding. *Toxicol Appl Pharmacol* 1996; **136:** 161-169.

21. Ronco P, Pollard H, Galceran M*, et al.* Distribution of enkephalinase (membrane metalloendopeptidase, E.C. 3.4.24.11) in rat organs. Detection using a monoclonal antibody. *Lab Invest* 1988; **58:** 210-217.

22. Lebeau C, Debelle FD, Arlt VM*, et al.* Early proximal tubule injury in experimental aristolochic acid nephropathy: functional and histological studies. *Nephrol Dial Transplant* 2005; **20:** 2321-2332.

23. Arlt VM, Zuo J, Trenz K*, et al.* Gene expression changes induced by the human carcinogen aristolochic acid I in renal and hepatic tissue of mice. *Int J Cancer* 2011; **128:** 21-32.

24. Moldovan GL, Pfander B, Jentsch S. PCNA, the maestro of the replication fork. *Cell* 2007; **129:** 665-679.

25. Debelle FD, Vanherweghem JL, Nortier JL. Aristolochic acid nephropathy: a worldwide problem. *Kidney Int* 2008; **74:** 158-169.

26. Yang L, Su T, Li XM*, et al.* Aristolochic acid nephropathy: variation in presentation and prognosis. *Nephrol Dial Transplant* 2011.

27. Chen CH, Dickman KG, Moriya M*, et al.* Aristolochic acid-associated urothelial cancer in Taiwan. *Proc Natl Acad Sci U S A* 2012.

28. Kwon O, Wang WW, Miller S. Renal organic anion transporter 1 is maldistributed and diminishes in proximal tubule cells but increases in vasculature after ischemia and reperfusion. *Am J Physiol Renal Physiol* 2008; **295:** F1807-1816.

29. Xue X, Gong LK, Maeda K*, et al.* Critical role of organic anion transporters 1 and 3 in kidney accumulation and toxicity of aristolochic acid I. *Mol Pharm* 2011; **8:** 2183-2192.

30. Nortier JL, Schmeiser HH, Muniz Martinez MC*, et al.* Invasive urothelial carcinoma after exposure to Chinese herbal medicine containing aristolochic acid may occur without severe renal failure. *Nephrol Dial Transplant* 2003; **18:** 426-428.

31. Dickman KG, Sweet DH, Bonala R*, et al.* Physiological and molecular characterization of aristolochic Acid transport by the kidney. *J Pharmacol Exp Ther* 2011; **338:** 588-597.

32. Balachandran P, Wei F, Lin RC*, et al.* Structure activity relationships of aristolochic acid analogues: toxicity in cultured renal epithelial cells. *Kidney Int* 2005; **67:** 1797-1805.

33. Stiborova M, Frei E, Schmeiser HH. Biotransformation enzymes in development of renal injury and urothelial cancer caused by aristolochic acid. *Kidney Int* 2008; **73:** 1209-1211.

34. Schmeiser HH, Stiborova M, Arlt VM. Chemical and molecular basis of the carcinogenicity of Aristolochia plants. *Curr Opin Drug Discov Devel* 2009; **12:** 141-148.

35. Qi X, Cai Y, Gong L*, et al.* Role of mitochondrial permeability transition in human renal tubular epithelial cell death induced by aristolochic acid. *Toxicol Appl Pharmacol* 2007; **222:** 105-110.

36. Hsin YH, Cheng CH, Tzen JT*, et al.* Effect of aristolochic acid on intracellular calcium concentration and its links with apoptosis in renal tubular cells. *Apoptosis* 2006; **11:** 2167-2177.

37. Yu FY, Wu TS, Chen TW*, et al.* Aristolochic acid I induced oxidative DNA damage associated with glutathione depletion and ERK1/2 activation in human cells. *Toxicol In Vitro* 2011; **25:** 810-816.

38. Li Y, Liu Z, Guo X*, et al.* Aristolochic acid I-induced DNA damage and cell cycle arrest in renal tubular epithelial cells in vitro. *Arch Toxicol* 2006; **80:** 524-532.

39. Chang HR, Lian JD, Lo CW*, et al.* Aristolochic acid-induced cell cycle G1 arrest in human urothelium SV-HUC-1 cells. *Food Chem Toxicol* 2007; **45:** 396-402.

40. Yang L, Besschetnova TY, Brooks CR*, et al.* Epithelial cell cycle arrest in G2/M mediates kidney fibrosis after injury. *Nat Med* 2010; **16:** 535-543, 531p following 143.

41. Phillips DH, Arlt VM. The 32P-postlabeling assay for DNA adducts. *Nat Protoc* 2007; **2:** 2772-2781.

42. Arlt VM, Zuo J, Trenz K*, et al.* Gene expression changes induced by the human carcinogen aristolochic acid I in renal and hepatic tissue of mice. *Int J Cancer* 2010.

ACKNOWLEDGMENTS

Part of the study was supported by Cancer Research, UK and by the Fonds Erasme pour la Recherche Médicale, Brussels Belgium. Preliminary data of this work have been accepted for presentation at the Annual Meeting of the Société de Néphrologie (October 5-7, 2011, Bordeaux, France), and at the Annual Meeting of the American Society of Nephrology (November 9-13, 2011, Philadelphia, USA).

LEGENDS TO THE FIGURES

Figure 1 | Schematic representation of experimental protocols performed in the mouse model of aristolochic acid nephropathy (AAN).

C57BL/6 male mice (*n*=96) were randomized in 4 groups of 24 mice each. AA (5 mg/kg body weight) was injected once a day and PBN (150 mg/kg body weight) twice a day. After 2, 4, 5 and 8 days of injection, six mice/group were sacrificed and blood sample and kidneys were harvested for further analysis.

Figure 2 | Evolution of plasma creatinine levels.

Plasma creatinine from AA (white columns), AA+PBN (grey columns) treated mice as compared to PEG+PBN (dashed columns) and PEG (dotted columns) controls from days 2 to 8. Results are presented as the mean ± SEM ; n = 6 mice/group. (**P<0.01)

Figure 3 | Histological analysis of tubulointerstitial injury in AA-treated mice compared to mice receiving AA+PBN.

Representative photomicrographs of renal cortex longitudinal sections at studied time points in each group. No lesions were observed in controls: PEG (**a-d**) and PEG+PBN (**e-h**). In AA group (**i-l**), tubular necrosis (arrow) was observed at days 4 and 5 in the outer stripe of outer medulla. In AA+PBN group (**m-p**), only sparse proximal tubules exhibited necrotic cells on day 4 (arrow) but lymphocytic infiltrate, tubular atrophy and interstitial fibrosis were absent on day 8. Original magnification x400, hematoxyllin-eosin stained kidney longitudinal sections.

Figure 4 | Histological analysis of tubulointerstitial injury in AA-treated mice

compared to mice receiving AA+PBN.

Representative photomicrographs of renal cortex longitudinal sections at studied time points in each group. No lesions were observed in controls: PEG (**a-d**) and PEG+PBN (**e-h**). In AA group (**i-l**), swelling of PTEC was observed after 2 days of injection (**$**), followed by tubular necrosis at days 4 and 5 (arrow). Tubular atrophy (star) and progressive interstitial fibrosis (arrowhead) were present after 8 days of injection. In AA+PBN group (**m-p**), tubular atrophy and interstitial fibrosis were absent on day 8. Original magnification x400, Goldner's trichrome stained kidney longitudinal sections.

Figure 5 | Semiquantitive tubulointerstitial score.

In control groups (PEG or PEG+PBN), no lesions were observed (data not shown). However, a significant increase in the necrosis score was observed in AA group (white columns) as soon as day 4 and was maximal on day 5 (**a**) as compared to controls. Tubular necrosis phase was followed by a significant lymphocytic infiltrate (**b**), atrophy (**c**) and fibrosis (**d**) respectively on day 8. A significant reduction of necrosis, atrophy and fibrosis was observed in the AA+PBN group (grey columns). Results are presented as the mean ± SEM, n= 6 mice/group. Significant levels are ** $P<0.01$.

Figure 6 | Representative photomicrographs of NEP staining in different groups and time.

In control groups (PEG (**a-b**) a NEP (neutral endopeptidase) positive staining was observed in medullary rays and in the outer stripe of outer medulla. An identical distribution was observed in PEG+PBN group (data not shown). However, in the AA group (**c-d**), a severe necrosis followed by a profound atrophy of PTECs was observed mainly in NEP positive area corresponding to S3 segment of proximal tubule. In the

AA+PBN group (**e-f**), necrosis was limited. (Original magnification: x200)

Figure 7 | Time course of AA-DNA adduct formation in renal tissue. Total AA-DNA adduct formation was determined by ^{32}P-postlabeling in AA (white columns) and AA+PBN groups (grey columns) in two separate experiments from 6 to 24 hours and from day 2 to day 8. As shown in **(a)**, the pattern of AA-DNA adducts consisted of three major adduct spots: 7-(deoxyadenosin-*N*^{6}-yl)- aristolactam I (dA-AAI; spot 1); 7-(deoxyguanosin-*N*^{2}-yl)-aristolactam I (dG-AAI; spot 2); and 7-(deoxyadenosin-*N*^{6}-yl)-aristolactam II (dA-AAII; spot 3). Results (**b**) are presented as the mean ± SEM n= 4 mice/group (6-24 hours) or n = 6 (2-8 days)/group. Significant levels are *p<0.05 and **P<0,01.

Figure 8 | Representative photomicrographs of PCNA staining in different groups and time points with quantification.

In control groups (PEG (**a-d**) and PEG+PBN (**e-h**)) only scattered PCNA positive PTEC were observed as compared to AA group (**i-l**) where numerous PCNA positive PTEC were present. Coadministration of PBN and AA (**m-p**) resulted in a substantial reduction of PCNA-positive PTEC on day 8. (Original magnification: x400) Quantification of positive PCNA cells (**q**) in AA (white columns), AA+PBN (grey columns), PEG+PBN (dashed columns) and PEG groups (dotted columns). Results are presented as the mean ± SEM; n= 6 mice/group. Significant levels are *P<0.05, **P<0.01.

Figure 9 | Representative electron photomicrographs from different groups on day 8.

Kidneys from PEG (Magnification x3000) (**a**) and PEG+PBN (Magnification x5000) (**b**)

groups : proximal tubules (£) are lined by tall columnar cells with acidophilic cytoplasm rich in structures necessary for active fluid transport : densely packed microvilli forming brush border, basal ondulations, endocytic vacuoles and mitochondria, often elongated and tortuous. In the AA group (Magnification x3000) (**c**), PTEC exhibited severe injury with disruption of brush border and cell detachment ($). In kidneys from the AA+PBN group (Magnification x3000) (**d**) PTEC displayed extensive cytoplasmic vacuolization without necrotic changes (**). Kidneys from the AA group, (x 30,000) (**e**) normal (£) and injured tubules were frequently admixed with injured nephron showing extensive mitochondria disruption (arrow head) and altered brush borders. AA+PBN group (Magnification x30,000) (**f**) displayed mitochondria vacualoziation (arrow head).

Figure 10 | Quantitative analysis of PCNA staining.

Twenty non-overlapping high power fields were photographed per section at a 400x magnification. Identical imaging conditions, including illumination intensity and camera exposure time, were applied to all photographs. A blankfield image was used to correct uneven illumination and color balance with the calculator Plus plugin. Then, brown-colored images specific for DAB stain and blue-colored images specific for hematoxylin stain were extracted by color deconvolution plugin. Nuclei generated from DAB images were isolated using specific threshold ImageJ internal commands followed by conversion to a binary image.

1 **FIGURES**

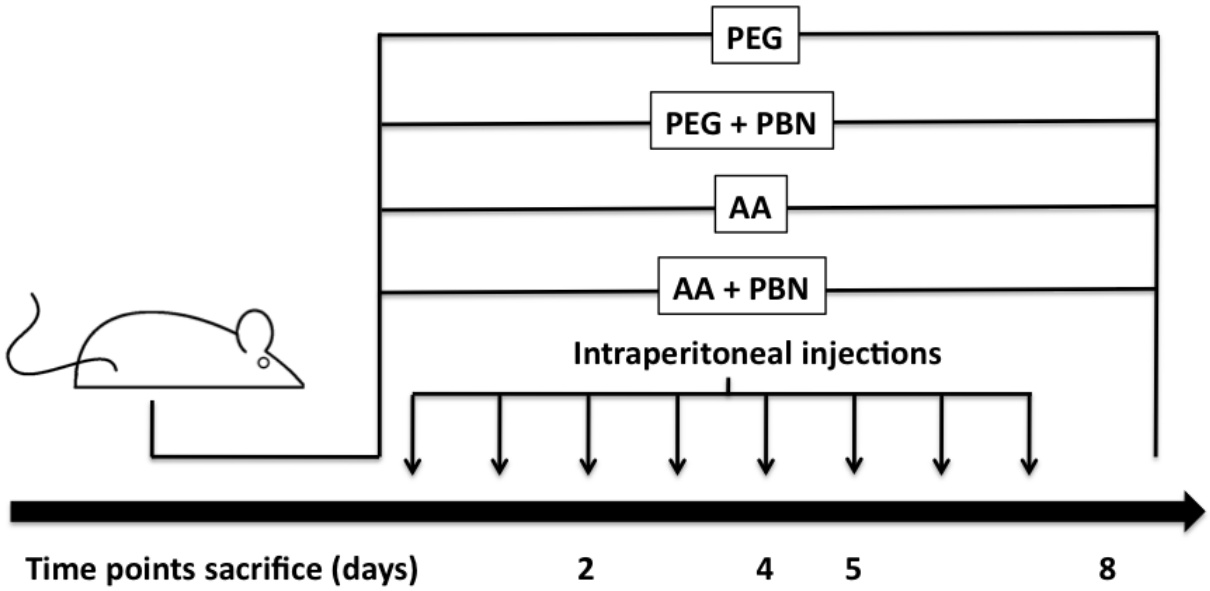

2
3 **Figure 1**
4

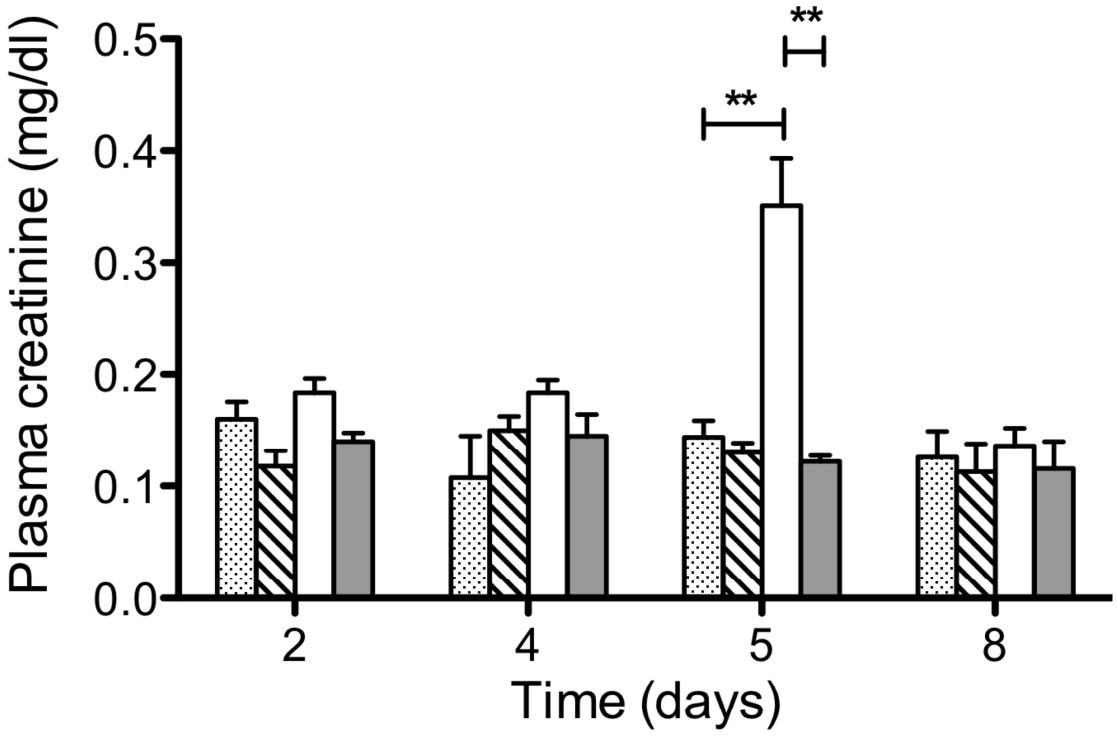

Figure 2

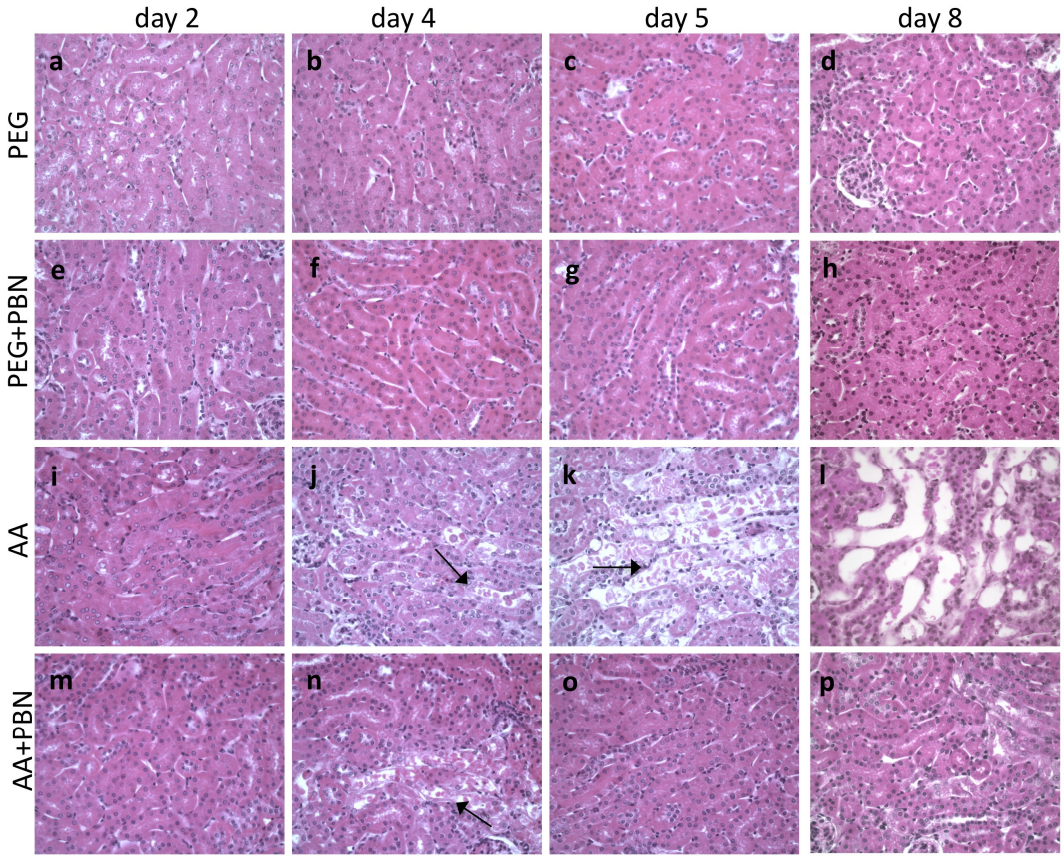

Figure 3

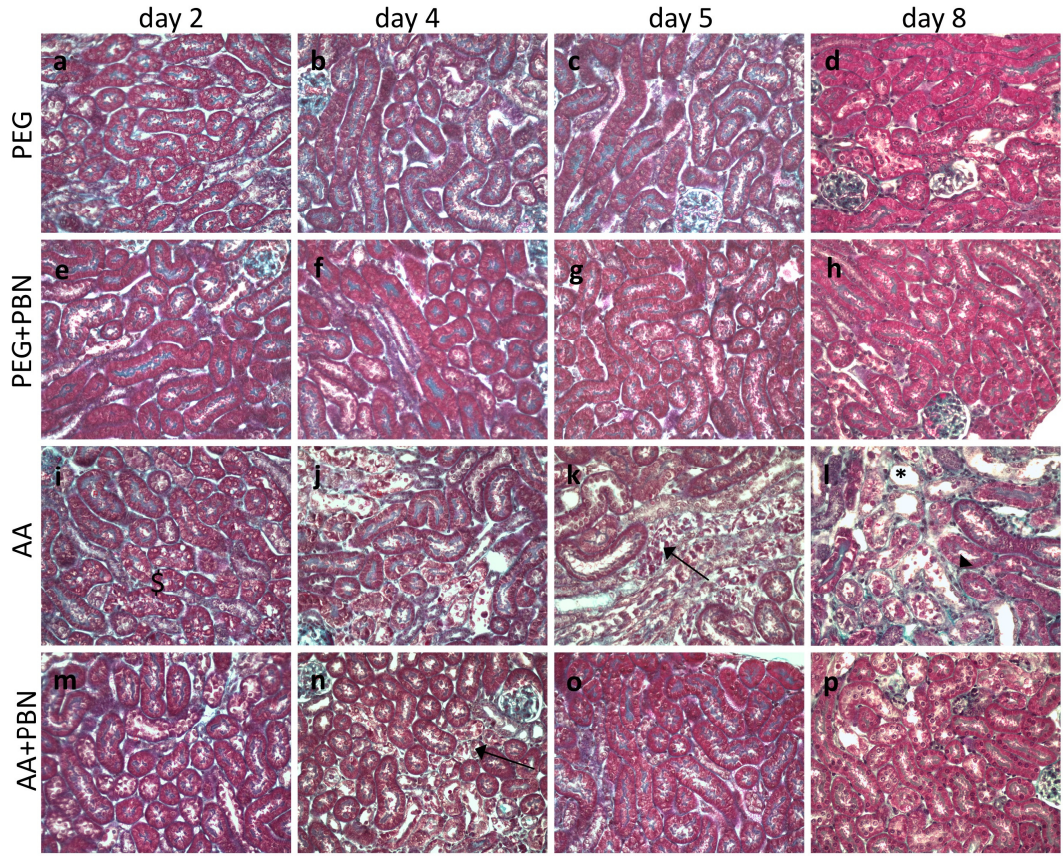

Figure 4

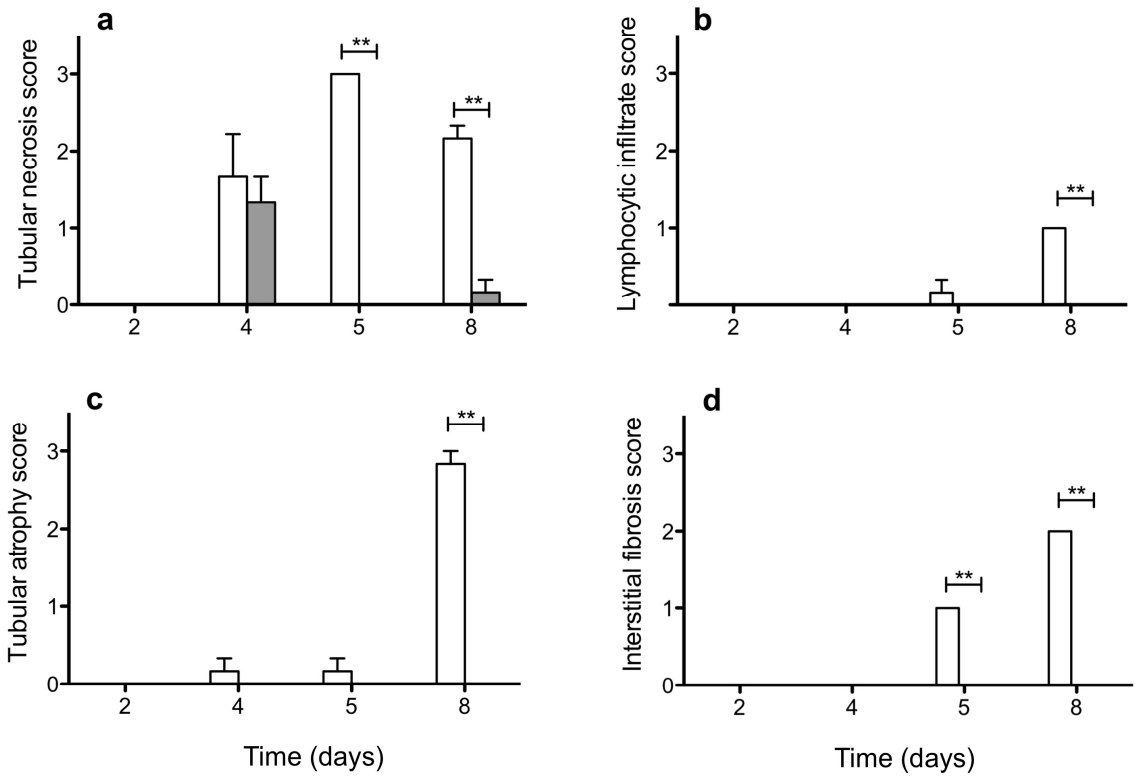
a
Tubular necrosis score
b
Lymphocytic infiltrate score
c
Tubular atrophy score
d
Interstitial fibrosis score
**
Time (days)
Time (days)

Figure 5

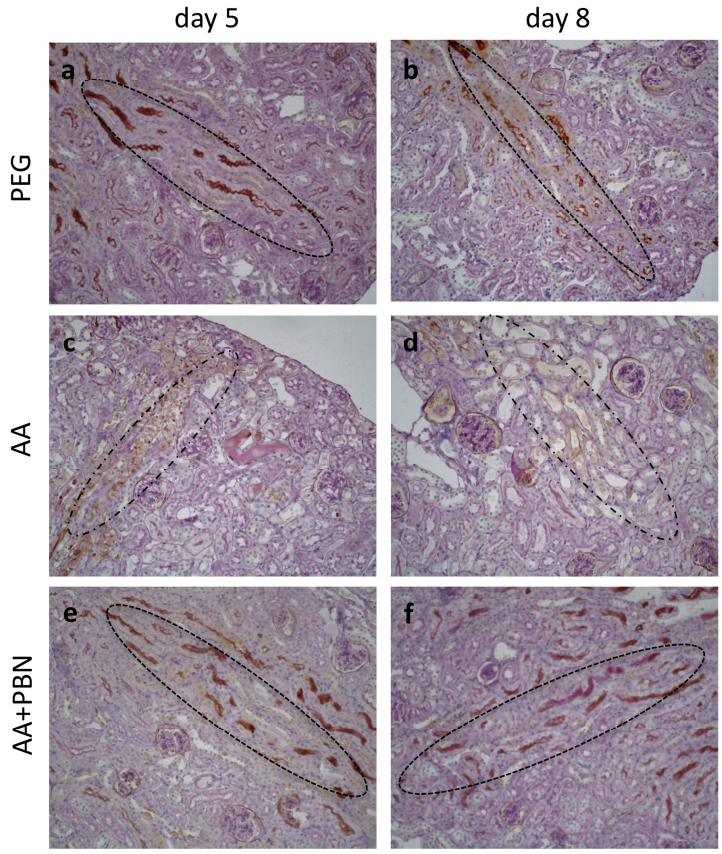

Figure 6

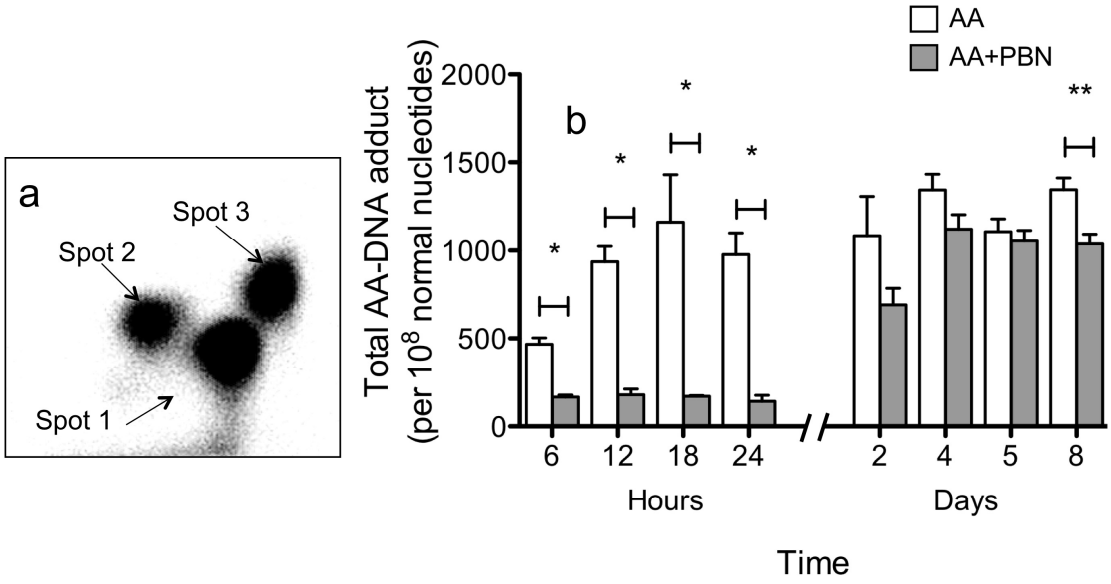
a
Spot 3
Spot 2
Spot 1
b
AA
AA+PBN
Total AA-DNA adduct
(per 10^8 normal nucleotides)
2000
1500
1000
500
0
*
*
*
*
**
6
12
18
24
2
4
5
8
Hours
Days
Time

Figure 7

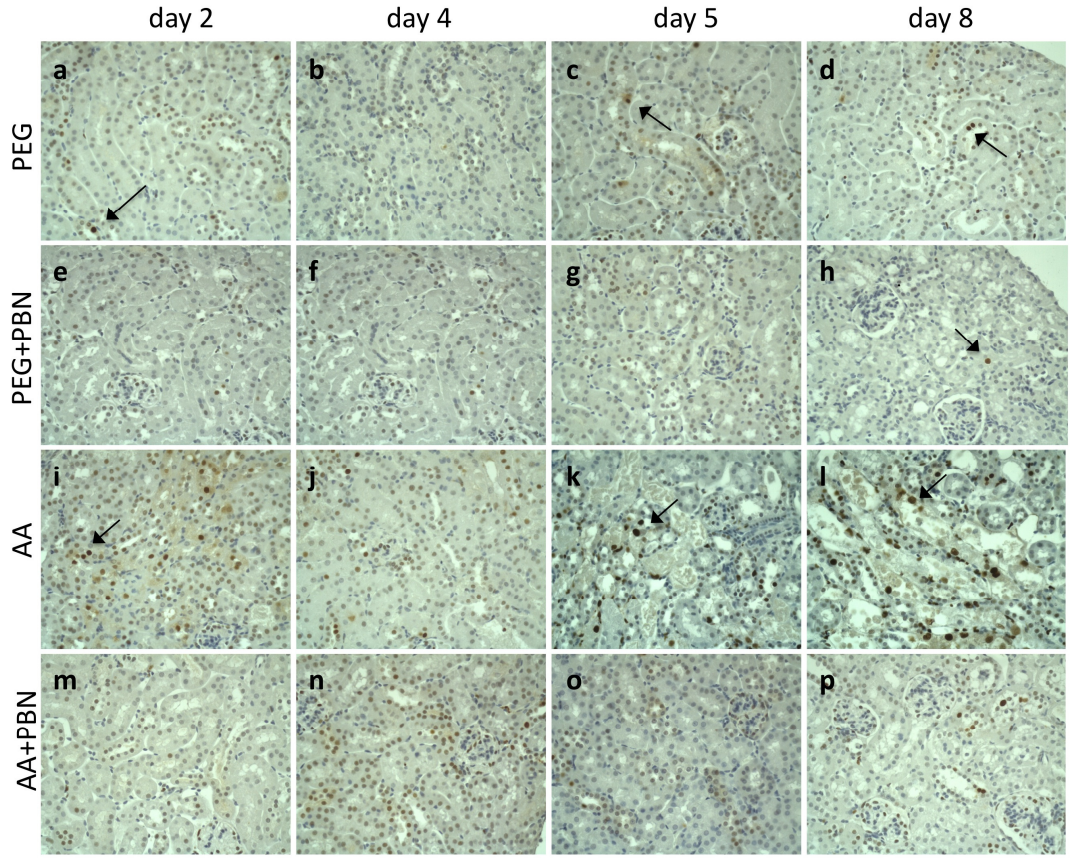
day 2
day 4
day 5
day 8
PEG
PEG+PBN
AA
AA+PBN
a
b
c
d
e
f
g
h
i
j
k
l
m
n
o
p

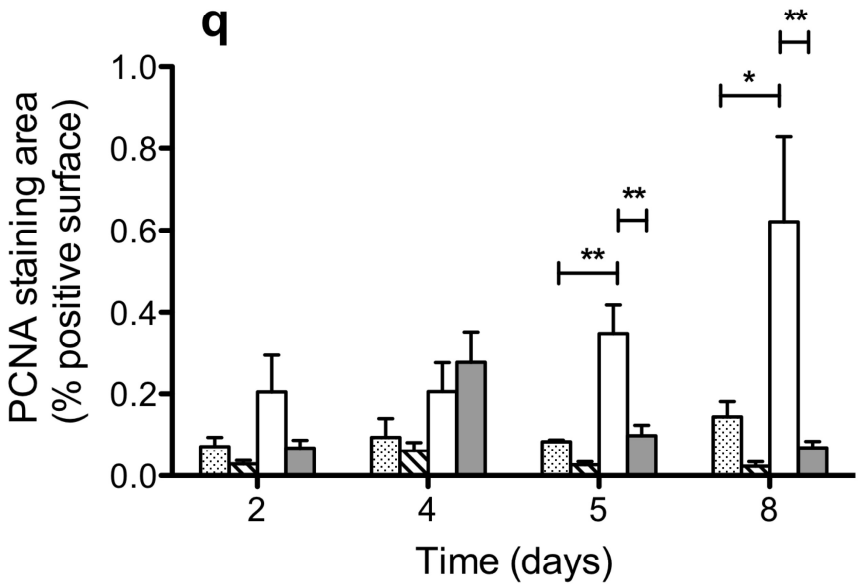
q
PCNA staining area
(% positive surface)
1.0
0.8
0.6
0.4
0.2
0.0
2
4
5
8
Time (days)
**
**
*
**

Figure 8

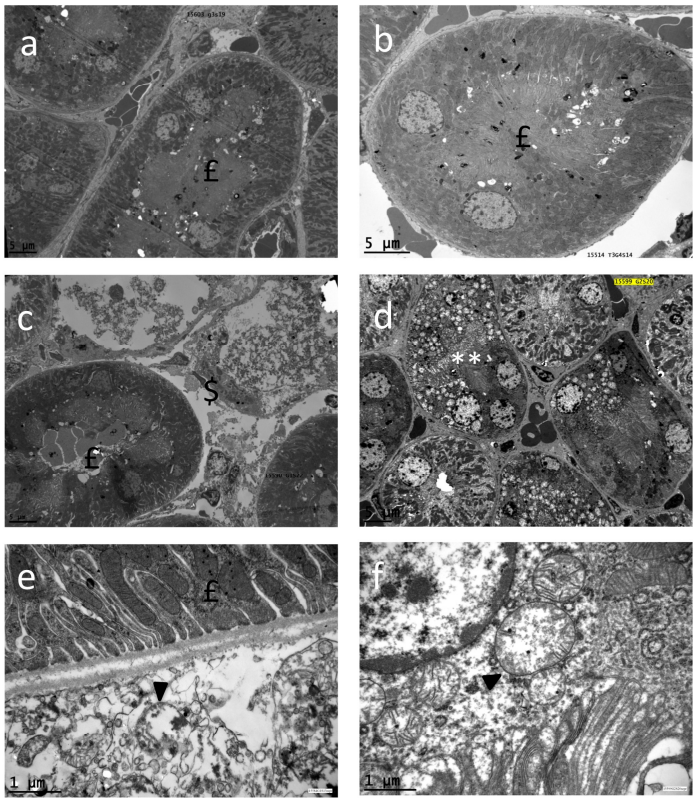

Figure 9

1

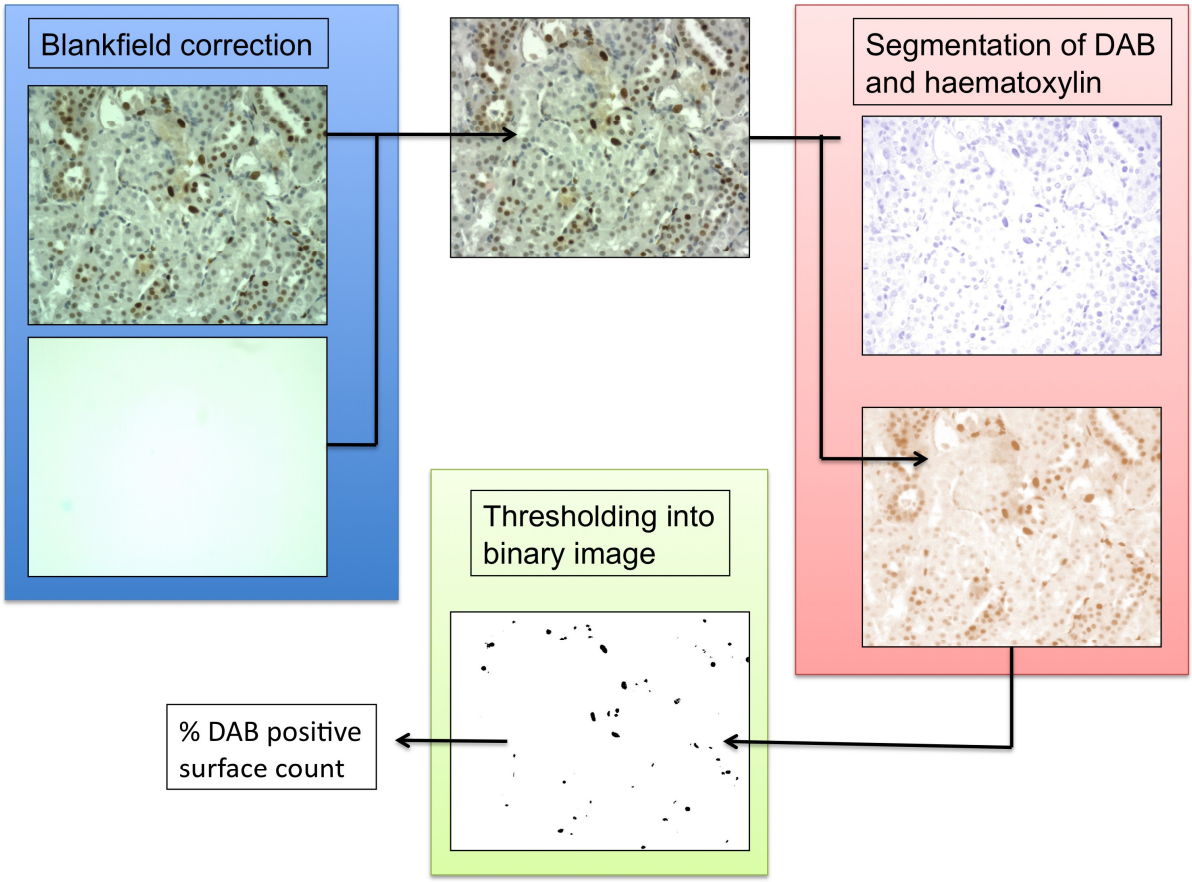

2
3
4
5
6

Figure 10